Desalination and Water Treatment
www.deswater.com
doi: 10.1080/19443994.2014.922440

55 (2015) 1007–1017
July

Taylor & Francis
Taylor & Francis Group

Utilization of oxalic acid-modified spent mushroom substrate for removal of methylene blue from aqueous solution

Tingguo Yan, Peng Wang, Lijuan Wang*

Key Laboratory of Bio-based Materials Science and Technology of Ministry of Education, Northeast Forestry University, 26 Hexing Road, Harbin 150040, P.R. China, Tel. +86 451 82191693; Fax: +86 451 82191693; email: donglinwlj@163.com

Received 3 October 2013; Accepted 5 May 2014

ABSTRACT

Spent mushroom substrate (SMS), an agricultural biowaste, was modified by oxalic acid and used as an adsorbent for adsorption of methylene blue (MB) in aqueous solution. The equilibrium data fitted with Freundlich and Temkin isotherm models. The kinetic experiment data followed the pseudo-second-order model. The experimental data corresponded well to Boyd's film-diffusion model and the rate-determining step was the external mass transfer. Thermodynamic parameters suggested that the adsorption process was exothermic and spontaneous. The results imply that OASMS is an economical and feasible adsorbent for removal of MB from aqueous solution.

Keywords: Adsorption; Methylene blue; Oxalic acid-modified spent mushroom substrate; Isotherm; Kinetics

1. Introduction

Synthesis dyes are extensively used in the textile, leather, cosmetics, paper, pharmaceutical, and food industries. It is reported that as much as 15% of the used dye is lost to the wastewater because of the low levels of dye-fiber fixation [1]. The release of dye-laden wastewaters from these industries has left a big threat on human beings and the environmental society due to the persistent and recalcitrant nature of dyes. Even just very low concentration of dyes could impart visible color to water body and reduce sunlight penetration and photosynthesis, which seriously destroy aquatic ecosystems [2]. Furthermore, most of dyes are toxic, carcinogenic, mutagenic, and teratogenic, which may cause severe damage to human beings and aquatic life [3]. Therefore, the removal of dye from wastewaters prior to their final discharge has been an important issue to be solved. Many dyes are stable to photodegradation, biodegradation, and oxidizing agents due to their complex aromatic molecular structure and synthetic origin [4,5]. Currently, the methods for dye-laden wastewaters treatment including coagulation, chemical oxidation, membrane separation process, electrochemical and, aerobic and anaerobic microbial degradation, are not very successful due to many restrictions [6]. Comparing with these methods, adsorption has been more preferred in applications [7]. Activated carbon has desirable adsorption capacity for most pollutants. However, the cost of activated carbon and the loss of adsorption efficiency after regeneration of the exhausted activated carbon have restricted its widespread application [8]. Therefore, a lot of interests have been paid to some low-cost and efficient adsorbents from agriculture biowaste. Many agriculture biowastes, such as wood chips [9], barley

*Corresponding author.

husk [10], sugar beet pulp [11], wheat husk [12], hazelnut shells [13], garlic peel [14], papaya seed [15], and sugarcane bagasse [16] were studied as economical and feasible adsorbents for removal of different dyes. However, many low-cost absorbents have relatively low adsorption capacity; thus, the consumption amounts are very huge. At present, the key studies are focused on finding new and economical adsorbents or improving adsorption capacity of those low-cost absorbents by chemical modification.

Spent mushroom substrate (SMS), an agricultural biowaste, is produced after being used for growing edible fungi. In China, the total SMS after the edible fungi cultivation has reached about 29 million tons annually, but most of them are disposed off with additional cost [17]. Hence, a proper treatment route to convert such kind of agricultural biowaste to useful end product would offset the costs of treatment and disposal [18]. In this study, SMS was modified by oxalic acid in order to improve the adsorption capacity. The effects of adsorbent dose, initial dye concentration, initial solution pH, contact time, and temperature on MB adsorption were investigated. Kinetics, isotherm, and thermodynamic parameters of the adsorption process were also investigated.

2. Materials and methods

2.1. Preparation of MB solutions

Methylene blue (MB) (MF, $C_{16}H_{18}ClN_3S{\cdot}3H_2O$; FW, 373.90; λ_{max}, 668 nm) and oxalic acid dihydrate were received from Tianjin Kemiou and Tianjin Hengxing Chemical Reagent Co., Ltd, respectively. The chemical structure of MB is displayed in Fig. 1. An aqueous stock solution of 500 mg L^{-1} dye was prepared by dissolving 0.5 g of MB in 1 L distilled water. The test solutions were obtained by dilution of stock solution to the desired concentration in a range from 40 to 100 mg L^{-1}. All reagents were of analytical reagent grade and used without further purification in this study.

2.2. Preparation of OASMS adsorbent

SMS was collected in summer 2010 from Taoshan town in the Yichun forest district of Heilongjiang Province, China. The collected materials were washed thoroughly with running water and then rinsed with distilled water several times to remove impurities. The clean SMS was put into an oven at 85 ℃ for 6 h. The dried SMS was crushed and sieved to 60–80 mesh particles. The required amount of dried SMS (60–80 mesh) was treated in 0.6 mol L^{-1} oxalic acid solution at 60 ℃ for 2 h. Then, the filtrate was removed and the residue was dried at 50 ℃ for 24 h and then dried at 120 ℃ for another 3 h. The OASMS was obtained and stored in airtight container for adsorption experiments.

2.3. Analytical measurements

A Nicolet 560 spectrometer (Nicolet Co., Ltd, USA) was employed to characterize the surface functional groups responsible for MB adsorption. The spectra were recorded in the range 4,000–400 cm^{-1}. Surface morphology of adsorbent before and after adsorption was observed using a Quanta 200 scanning electron microscope with an accelerating voltage of 12.5 kV. The aqueous solutions' pHs were measured by digital pH meter (PHSJ-4F). The unknown concentration of MB solution in adsorption process was determined using UV-visible spectrophotometer by monitoring the absorbance changes at λ_{max} 668 nm.

2.4. Adsorption experiments

The batch adsorption experiments for evaluating the potential of OASMS for MB adsorption were conducted in 250 mL conical flasks containing 50 mL MB solutions in a water bath. The conical flasks were shaken at 110 rpm for the required time. The effect of solution pH on MB adsorption onto OASMS was investigated in the pH range from 2 to 10. The pH of each solution was adjusted to the required value with

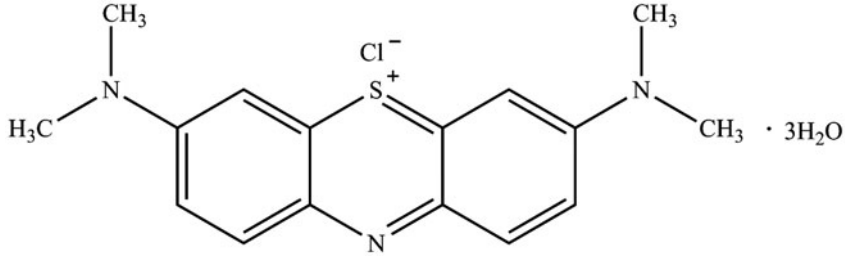

Fig. 1. The chemical structure of MB in hydrated form.

HCl or NaOH solutions prior to the addition of OASMS adsorbent.

In the present study, adsorption equilibrium experiments were carried out by stirring an 80 mg L^{-1} solution of MB dye with various adsorbent doses from 30 to 200 mg at original solution pH. The solutions were agitated and maintained at different temperatures ranging from 303 to 333 K for 12 h. Adsorption kinetic experiments were performed by using 100 mg of OASMS and 80 mg L^{-1} solution of MB dye. The system was stirred at various temperatures ranging from 303 to 333 K. Then, the flasks were taken out at some intervals. At the end of each adsorption experiment, the adsorbent was removed by filtration through a 400 mesh nylon screen. The dye concentration of the supernatant was measured by UV-visible spectrophotometer. The dye removal (R, %), and the amount of MB dye adsorbed at time t (q_t, mg g^{-1}), and at equilibrium (q_e, mg g^{-1}), were calculated using the following equations:

$$R\ (\%) = [(C_0 - C_t)/C_0] \times 100 \tag{1}$$

$$q_t = (C_0 - C_t)V/W \tag{2}$$

$$q_e = (C_0 - C_t)V/W \tag{3}$$

where C_t (mg L^{-1}) is the dye concentration at time t, C_0 and C_e (mg L^{-1}) are the initial and equilibrium dye concentrations, respectively. q_e (mg g^{-1}) represents amounts of dye adsorbed per unit mass of adsorbent at equilibrium. V (mL) is the volume of the dye solution, and W (mg) is the weight of adsorbent.

2.5. Kinetics of the adsorption

The kinetic of sorption is an important characteristic in evaluating the efficiency of sorption process. Several kinetic models are available to describe the adsorption kinetics. Mostly used models such as pseudo-first order [19], pseudo-second order [20], intra-particle diffusion model [21], and Boyd's film-diffusion model [22] were tested for the sorption of MB onto OASMS.

2.5.1. Pseudo-first-order model

Pseudo-first-order equation proposed by Lagergren was to be used for elucidating the rate of adsorption and can be defined as follows:

$$\ln\ (q_e - q_t) = \ln\ q_e - k_1 t \tag{4}$$

where q_t (mg g^{-1}) and q_e (mg g^{-1}) is the amounts of MB adsorbed per unit weight of OASMS at time t (min) and at equilibrium, respectively. k_1 (min^{-1}) is the pseudo-first-order rate constant.

2.5.2. Pseudo-second-order model

Pseudo-second-order model is represented with the following equation:

$$t/q_t = 1/(k_2 q_e^2) + t/q_e) \tag{5}$$

where k_2 (g mg^{-1} min^{-1}) is the pseudo-second-order rate constant.

2.5.3. Intra-particle diffusion model

The intra-particle diffusion model proposed by Weber and Morris can be described as follows:

$$q_t = k_{id} t^{1/2} + C \tag{6}$$

where k_{id} (mg g^{-1} $min^{-1/2}$) is the intra-particle diffusion rate constant. C (mg g^{-1}) is a constant. According to this model, the plots of q_t vs. $t^{1/2}$ at different temperatures should produce a straight line if intra-particle diffusion is involved in the adsorption process and should pass through the origin if intra-particle diffusion is the rate-controlling step [23,24].

2.5.4. Boyd's film-diffusion model

The Boyd's film-diffusion model was employed to investigate the contribution of film resistance to the kinetics of MB adsorption. It assumes that the boundary layer surrounding the adsorbent particle is the main resistance to diffusion. The linear forms of film-diffusion model are obtained by Reichenberg [25]. Eq. (7) is used for values of $F(t)$ from 0 to 0.85 and Eq. (8) for values from 0.86 to 1.

$$B_t = 2\pi - \pi^2 F(t)/3 - 2\pi(1 - \pi F(t)/3)^{1/2} \tag{7}$$

$$B_t = -0.4977 - \ln\ (1 - F(t)) \tag{8}$$

$$F(t) = q_t/q_e \tag{9}$$

where q_e (mg g^{-1}) and q_t (mg g^{-1}) are the adsorption capacities at equilibrium and at time t (min), respectively. $F(t)$ represents the fraction of solute adsorbed at any time t (min), and Bt is a mathematical function of $F(t)$.

2.6. Isotherms of the adsorption

Adsorption isotherms describe the relationship between the concentrations of the adsorbate on the solid phase and in the liquid phase after the adsorption system attained equilibrium at a constant temperature. The isotherm parameters calculated from the equilibrium models give insight into the adsorption mechanism, surface properties, and affinity of the adsorbent with the adsorbate [26]. In this study, the equilibrium data were fitted by Langmuir [27], Frundlich [28], and Temkin [29] isotherm model, respectively.

2.6.1. Langmuir isotherm

The Langmuir isotherm model suggests that all sites within the adsorbent are energetically equivalent, the interaction between molecules adsorbed on neighboring sites can be negligible, and the adsorbent surface is saturated after monolayer adsorption [30]. The linear form is expressed as:

$$C_e/q_e = 1/(bqm) + C_e/q_m \tag{10}$$

where C_e (mg L^{-1}) is equilibrium dye concentration. q_e (mg g^{-1}) represents amount of dye adsorbed onto adsorbent at equilibrium. q_m (mg g^{-1}) and b (L mg^{-1}) are the maximum monolayer capacity of the adsorbent and the Langmuir isotherm constant, respectively.

2.6.2. Freundlich isotherm

The Freundlich model suggests a multilayer sorption. It can be described as follows:

$$\ln q_e = \ln K_f + (1/n_f) \ln C_e \tag{11}$$

where K_f ((mg g^{-1})(mg $L^{-1})^{-1/n}$) is the Freundich constant and $1/n_f$ (dimensionless) is the heterogeneity factor.

2.6.3. Temkin isotherm

It assumes that the heat of adsorption of all molecules in the layer decreases linearly with coverage due to interactions among adsorbates and a uniform distribution of binding energies are used to characterize adsorption. It can be shown in linear form as follows:

$$q_e = (RT/b_T) \ln A_T + (RT/b_T) \ln C_e \tag{12}$$

where A_T (L g^{-1}) and b_T (J mol^{-1}) are the equilibrium constant corresponding to the maximum binding energy and a constant related to the heat of adsorption, respectively.

2.7. Thermodynamics of the adsorption

The thermodynamic data reflect the feasibility and favorability of the adsorption. The parameters such as free energy change, enthalpy change, and entropy change can be estimated by the change of equilibrium constants with temperature. These parameters are determined by the following equations:

$$\Delta G^0 = \Delta H^0 - T\Delta S^0 \tag{13}$$

$$\ln K_c = -(\Delta H^0/RT) + \Delta S^0/R \tag{14}$$

$$K_c = C_s/C_e \tag{15}$$

where ΔG^0 (kJ mol^{-1}), ΔH^0 (kJ mol^{-1}) and ΔS^0 (J mol^{-1} K^{-1}) are standard free energy change, enthalpy change, and entropy change, respectively. K_c and C_s (mg L^{-1}) are the equilibrium constant and the amount adsorbed on solid at equilibrium, respectively.

3. Results and discussion

3.1. Characterization of adsorbent

3.1.1. Fourier-transform infrared analysis

The infrared spectra of SMS (a) and OASMS (b) are shown in Fig. 2. As illustrated in Fig. 2(a) and (b), broad bands in the 3,200–3,600 cm^{-1} region are found, which can be presumably contributed by the overlapping stretches of N–H, O–H, and =C–H aromatic groups [31]. The characteristic alkyl C–H peaks are observed in a range from 2,800 to 3,000 cm^{-1} [32]. The strong peak at around 1,630 cm^{-1} is due to C=C stretching vibration. The peak at 1,321 cm^{-1} can be ascribed to C–O vibration in syringyl derivatives. The peak observed at 1,035 cm^{-1} can be assigned to C–O stretching in cellulose. Compared with the spectrum of SMS, the new peaks, 2,800–2,900 and 1,670–1,760 cm^{-1}, are found in Fig. 2(b), which are attributed to C–H stretching vibrations of carbonyl group and stretching vibrations of carbonyl groups in carboxylic acids, respectively [33]. The results show a number of carboxyl groups have been grafted onto SMS after modification by oxalic acid.

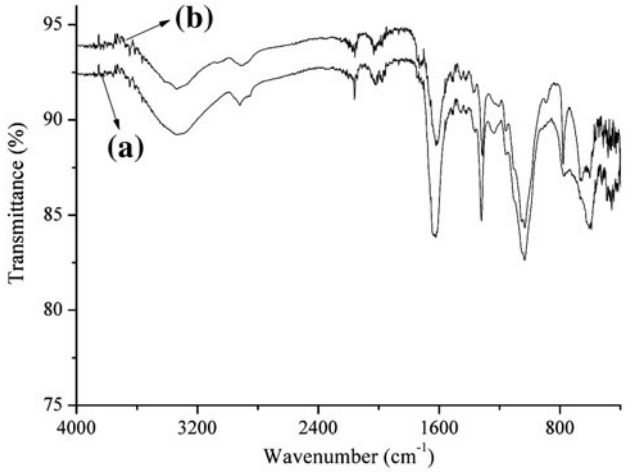

Fig. 2. Fourier-transform infrared (FT-IR) spectra of SMS (a) and OASMS (b).

3.1.2. Scanning electron microscopy observation

The Scanning electron microscopy (SEM) micrographs of SMS before and after modification by oxalic acid are given in Fig. 3(a) and (b), respectively. SMS consists of many natural polymers, such as lignin, cellulose, and hemicellulose, which are carbon and energy source for the fungus. As illustrated in Fig. 3(a), pores in SMS are left after these biopolymers being degraded and consumed by the fungus. Compared to SMS, it is found that the surface texture of OASMS changes since modification by oxalic acid occurs.

3.2. Effect of initial pH

As shown in Fig. 4, the effect of pH on adsorption capacity and removal of MB dye using OASMS adsorbent was investigated in the pH range of 2–10. There is an increase in both equilibrium adsorption capacity and removal of MB dye at pH from 2 to 4. Further increase of pH cannot obviously improve the removal and the adsorption capacity. MB dye is positively charged in water solution. The surface of OASMS adsorbents are surrounded by hydronium ions and the carboxyl groups were harder to ionize at pH below 4, which prevents the adsorption of MB dye ions onto OASMS surface owing to electrostatic repulsion and the competition between hydronium ions and MB dye ions for the adsorption sites [34]. The grafted carboxylic groups on OASMS surface are more easily deprotonated at higher pH, resulting in an increase in MB adsorption because of electrostatic attraction between $-COO^-$ and cationic dye [35]. However, the slight changes of removal and adsorption capacity at the pH range of 4–10 can be attributed to electrostatic attraction which was not the only mechanism for MB dye adsorption in this system. The OASMS can also interact with MB molecules via hydrogen bonding.

3.3. Effect of contact time and initial concentration

The effects of initial dye concentration and contact time on MB adsorption using OASMS adsorbent were investigated with various dye concentrations and intervals as depicted in Fig. 5. Most of MB dye was removed within the first 60 min. Equilibrium was achieved in 120 min at a concentration of 100 mg L^{-1} and then no more MB dye was adsorbed. Similar observations are found at other concentrations studied in this work. This is associated with large numbers of vacant active surface sites on OASMS surface that are available at the initial stage of the adsorption.

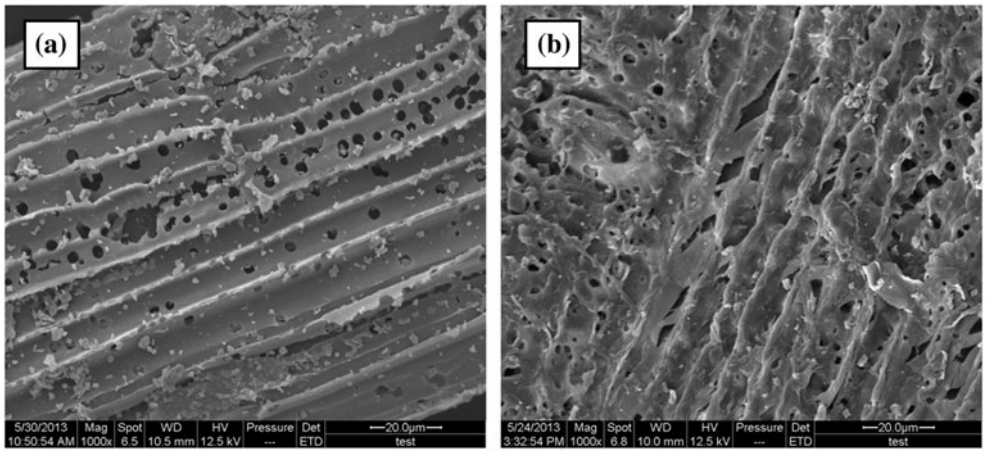

Fig. 3. SEM micrographs of SMS before (a) and after (b) modification.

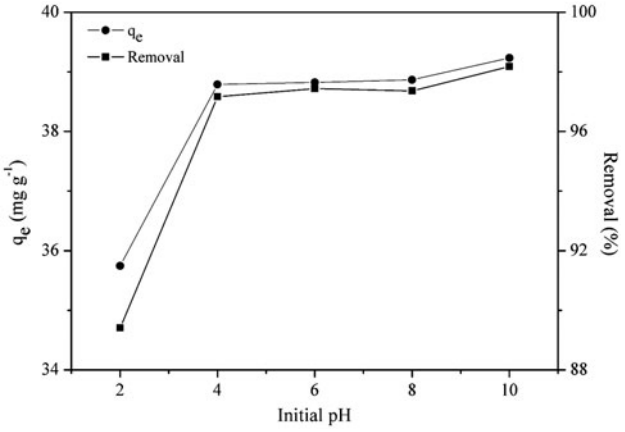

Fig. 4. Effect of initial solution pH on MB adsorption using OASMS adsorbent (dye concentration: 80 mg L^{-1}, volume: 50 mL, temperature: 303 K; dose: 100 mg; time: 12 h).

However, the remaining vacant active sites are less available for adsorption as the time lapsed and the repulsive forces occurring between the adsorbed and free molecules [36]. With the increasing initial MB concentration ranging from 40 to 100 mg L^{-1}, the adsorption capacity at equilibrium increases from 19.6 to 48.2 mg g^{-1} due to an increase in driving force for the mass transfer among the adsorbent and the adsorbate [34].

3.4. Effect of OASMS dose

The effects of OASMS dosage on MB dye adsorption were conducted by varying the adsorbent dose from 25 to 200 mg and temperatures from 303 to 333 K as shown in Fig. 6. It is found that the equilibrium adsorption capacity decreases from 128.2 to 19.7 mg g^{-1} with increasing adsorbent dose from 25 to 200 mg at 303 K. This can be attributed to the increased adsorbent surface area, i.e. the high number of unsaturated adsorption sites occurs during adsorption process [26]. Similar trends are found at other temperatures studied.

3.5. Effect of temperature

The effects of temperature on MB adsorption using OASMS were performed by varying the temperatures from 303 to 333 K as presented in Fig. 7. With the decreasing temperature, the equilibrium removal increases from 89.3 to 97.2% and the equilibrium adsorption capacity increases from 35.7 to 38.8 mg g^{-1}, revealing the exothermic nature of the MB dye adsorption on OASMS, i.e. lower temperatures favored the adsorption.

3.6. Study of adsorption parameters

3.6.1 Kinetic parameters

The linear plots of ln ($q_e - q_t$) vs. t and t/q_t against t are illustrated in Fig. 8. The values of k_1, k_2, and q_e at different temperatures can be determined from the slope and intercept of the plots. As listed in Table 1, the correlation coefficients (R^2) for the pseudo-first-order kinetic model are less than 0.854, and the calculated q_e ($q_{e,\text{cal.}}$) values are far lower than the experimental values of q_e ($q_{e,\text{exp.}}$). However, the $q_{e,\text{cal.}}$ for the

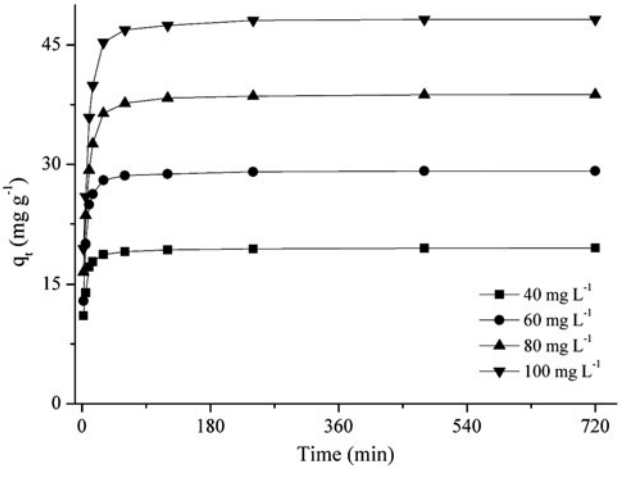

Fig. 5. Effect of initial dye concentration and contact time on MB adsorption (adsorbent dose: 100 mg, volume: 50 mL, temperature: 303 K).

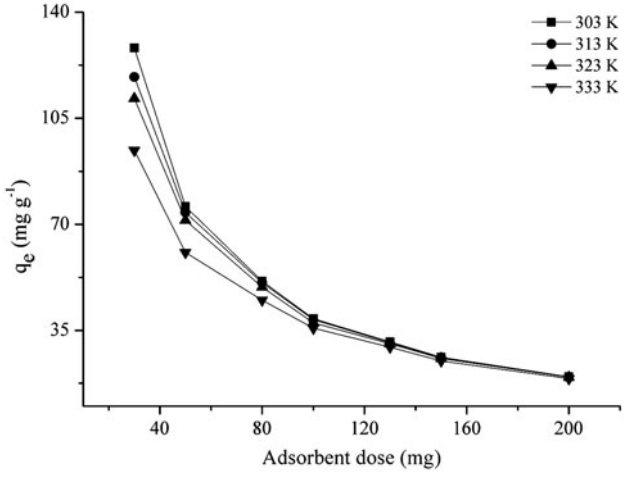

Fig. 6. Effect of adsorbent dose on MB adsorption (dye concentration: 80 mg L^{-1}, volume: 50 mL, time: 12 h).

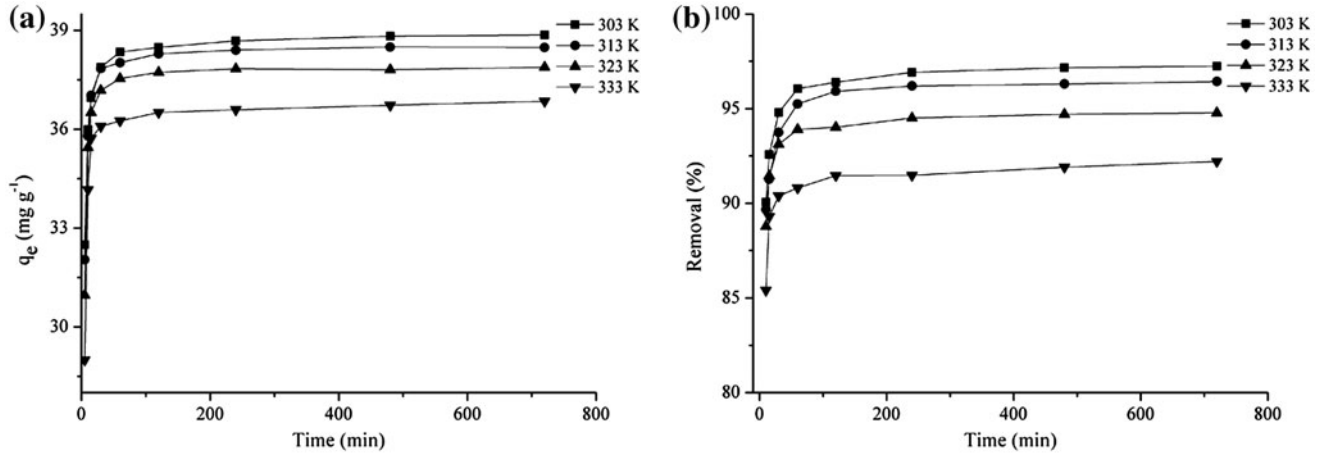

Fig. 7. Effect of temperature on the adsorption of MB dye using OASMS adsorbent (dye concentration: 80 mg L^{-1}, adsorbent dose: 100 mg, volume: 50 mL).

pseudo-second-order kinetic model is very close to the values of $q_{e,\text{exp.}}$ and all the R^2 values at different temperatures are 1.000, which indicates the experimental data can fit the pseudo-second-order model well.

As illustrated in Fig. 9(a), a multi-linear nature of the plot of the intra-particle diffusion model indicates that there are three steps with different rate constants affecting the adsorption process. The graphical analysis is applied for each linear region. The values of k_{id} and C are obtained from the slopes and intercepts of the plots and summarized in Table 2. In this work, the three regions lies in the range of 5–15 min, 15–60 min, and 60–720 min, respectively. It is found that the intra-particle diffusion rate constant (k_{id}) decreased with increasing time at 303 K, indicating that the intra-diffusion slowed down. The value of C obtained from the first linear region at 303 K is 26.56, which is significantly different from zero. This indicates that the adsorption rate in the first linear region at 303 K is not governed by intra-particle diffusion, i.e. the intra-particle diffusion is not the sole rate-controlling step. Similar trends and observations occur at other temperatures studied.

The Boyd plots of Bt against t for the MB adsorption at different temperatures are shown in Fig. 9(b). The Boyd parameters are listed in Table 2 with correlation coefficients (R^2) higher than 0.901. Fig. 9(b) clearly states that the film-diffusion is the controlling factor in the adsorption process since the plots of Boyd's film-diffusion model are linear and do not pass through the origin [37]. The fact that film diffusion played a major role in the adsorption processes

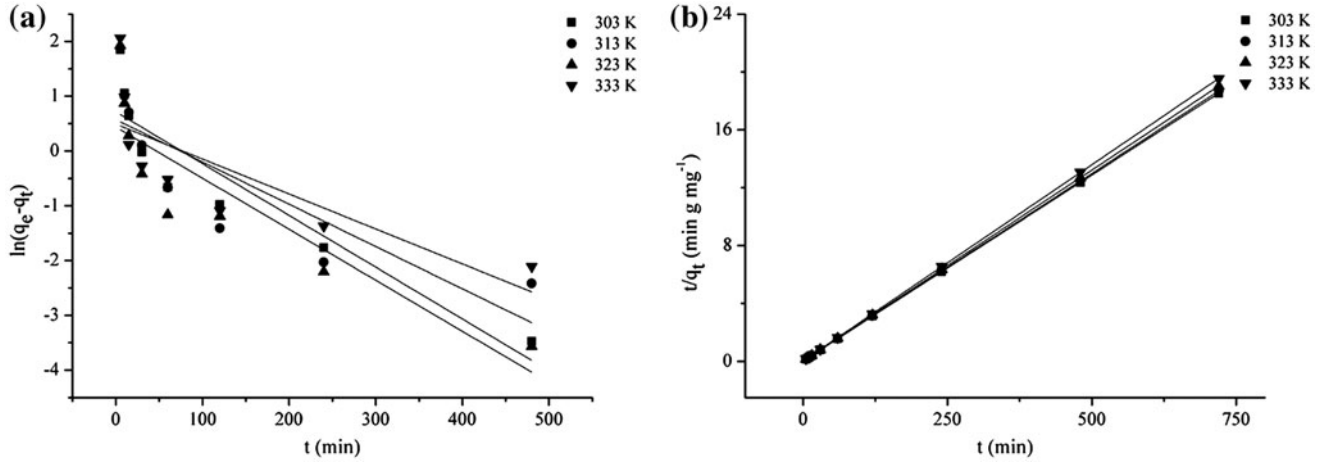

Fig. 8. The linear plots of pseudo-first-order (a) and pseudo-second-order (b) model.

Table 1
The pseudo-first-order and pseudo-second-order parameters

Model	Parameters	Temperature (K)			
		303	313	323	333
	$q_{e,\text{exp.}}$(mg g^{-1})	38.86	38.54	37.84	36.85
Pseudo-first order	k_1 (min^{-1})	0.0095	0.0077	0.0093	0.0064
	$q_{e,\text{cal.}}$ (mg g^{-1})	2.05	1.77	1.55	1.64
	R^2	0.854	0.698	0.780	0.626
Pseudo-second order	k_2 (g mg^{-1} min^{-1})	0.0266	0.0281	0.0340	0.0262
	$q_{e,\text{cal.}}$ (mg g^{-1})	38.91	38.61	37.88	36.90
	R^2	1.000	1.000	1.000	1.000

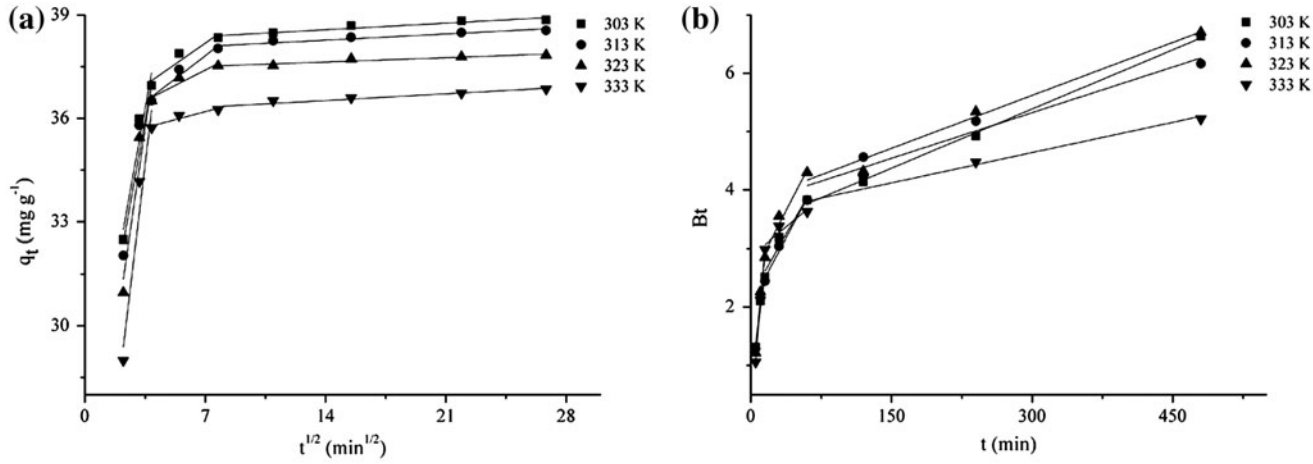

Fig. 9. The linear plots of intra-particle diffusion (a) and Boyd's film-diffusion (b) model.

Table 2
The intra-particle diffusion and Boyd's film-diffusion parameters

Model	Parameters	Temperature (K)			
		303	313	323	333
Intra-particle diffusion	k_{id1} (mg g^{-1} min$^{-1/2}$)	2.7782	2.7977	3.4591	4.1859
	C (mg g^{-1})	26.56	26.14	23.62	20.02
	R^2	0.943	0.913	0.931	0.950
	k_{id2} (mg g^{-1} min$^{-1/2}$)	0.3483	0.3824	0.2546	0.1326
	C (mg g^{-1})	35.743	35.139	35.619	35.265
	R^2	0.918	0.954	0.925	0.907
	k_{id3} (mg g^{-1} min$^{-1/2}$)	0.0274	0.0257	0.0178	0.0278
	C (mg g^{-1})	38.186	37.908	37.386	36.126
	R^2	0.927	0.914	0.912	0.919
Boyd's film-diffusion	Intercept (1)	0.7791	0.8011	0.4721	0.1242
	R^2	0.968	0.928	0.975	0.997
	Intercept (2)	2.1984	2.0598	2.4789	2.8676
	R^2	0.960	0.987	0.971	0.901
	Intercept (3)	3.3581	3.7589	3.8056	3.6022
	R^2	0.998	0.955	0.982	0.946

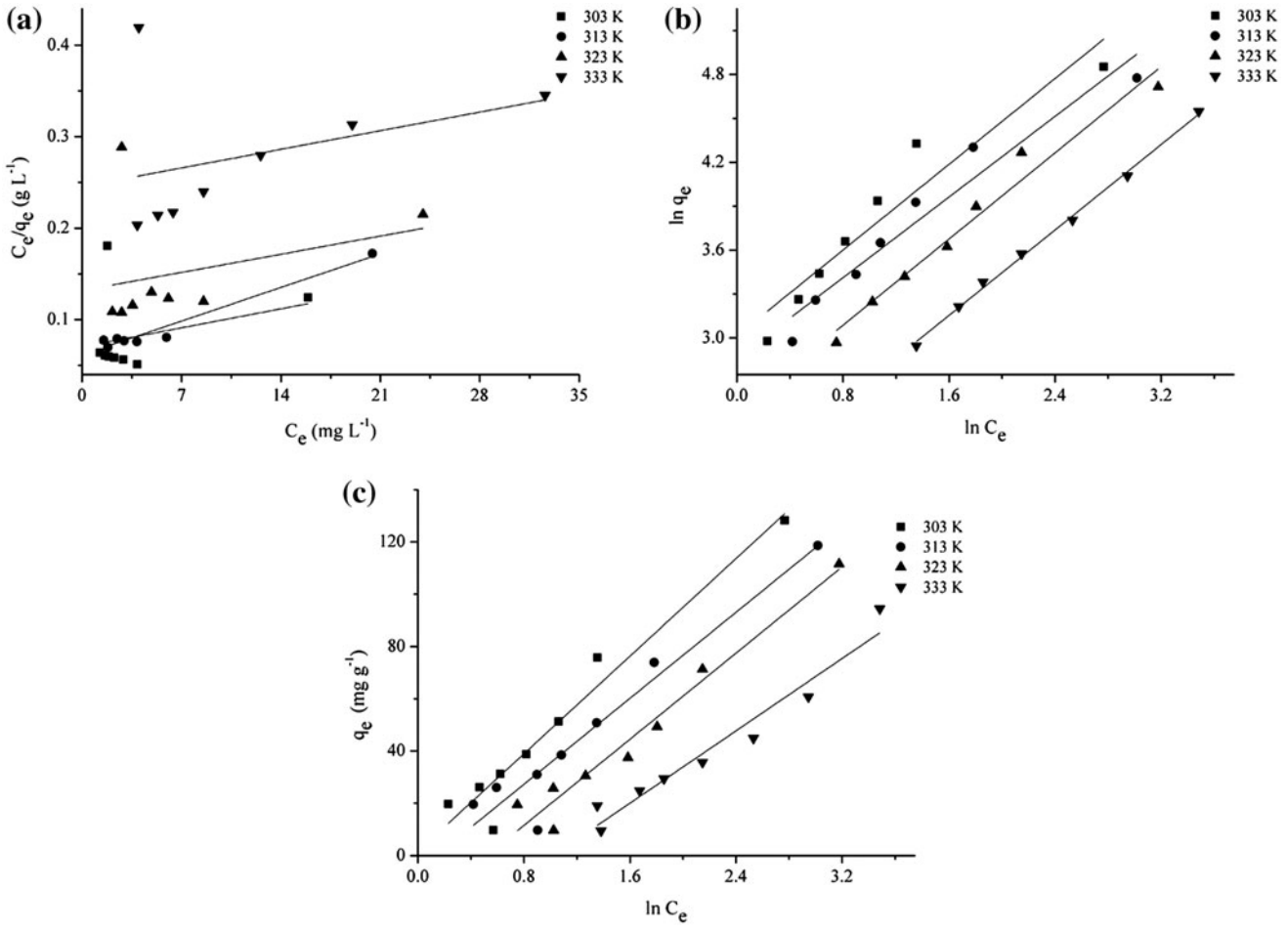

Fig. 10. The linear plots of Langmuir (a), Freundlich (b), and Temkin (c) equilibrium model.

suggested that the dye ions mainly bonded with the carboxylic groups on the surface of the adsorbents via the covalent bonds.

3.6.2. Isotherm parameters

The plot of C_e/q_e vs. C_e gives a linear relationship as shown in Fig. 10(a). b and q_m were calculated from the intercept and slope, and their values were listed in Table 3. The values of correlation coefficient (R^2) are in the range from 0.897 to 0.964. Therefore, the Langmuir model does not describe the MB adsorption well.

Fig. 10(b) shows the plot of ln q_e against ln C_e. $1/n_f$ and K_f can be calculated from the slope and intercept of the plot, respectively. The results are presented in Table 3. The correlation coefficients (R^2) are higher than 0.912, indicating that the experimental data can be described by the Freundlich model. The $1/n_f$ values at different temperatures are less than 1, illustrating that the MB adsorption on OASMS is favorable [38].

The values of A_T and b_T can be calculated from the intercept and the slope of the linear plots obtained by plotting q_e vs. ln C_e in Fig. 10(c). The results are listed in Table 3. The correlation coefficients (R^2) are higher than 0.941, which indicates the equilibrium data fitted the Temkin isotherm well.

3.6.3. Thermodynamic parameters

The values of ΔH^0 and ΔS^0 are calculated from the slope and intercept of a linear plot of ln K_c against $1/t$ and summarized in Table 4. The negative value of ΔH^0 confirms the exothermic nature of adsorption. The negative values of ΔG^0 at different temperatures (303–333 K) suggest the spontaneous nature of MB adsorption. The negative value of ΔS^0 suggests the decreased randomness at the solid/solution interface during the adsorption of MB dye on OASMS adsorbent.

Table 3
Equilibrium parameters for MB adsorption on OASMS

Model	Parameters	Temperature (K)			
		303	313	323	333
Langmuir	q_m (mg g^{-1})	217.4	188.7	208.3	196.1
	b (L mg^{-1})	0.095	0.087	0.096	0.026
	R^2	0.897	0.964	0.948	0.921
Freundlich	$1/n_f$	0.732	0.689	0.736	0.729
	K_f (mg g^{-1})(mg L^{-1})$^{-1/n}$	20.39	17.48	12.17	7.30
	R^2	0.912	0.947	0.971	0.997
Temkin	A_T (L mg^{-1})	1.153	0.998	0.654	0.377
	b_T (J mol^{-1})	56.43	66.30	68.24	82.01
	R^2	0.986	0.990	0.973	0.941

Table 4
Thermodynamic parameters for MB adsorption

R^2	ΔH^0 (kJ mol^{-1})	ΔS^0 (J mol^{-1} K^{-1})	ΔG^0 (kJ mol^{-1})			
			303 K	313 K	323 K	333 K
0.9836	−30.78	−71.43	−9.12	−8.41	−7.69	−6.98

4. Conclusions

In this study, OASMS was applied to MB adsorption from aqueous solution. Bath experiments by varying conditions such as adsorbent dose, initial dye concentration, initial solution pH, and temperature were conducted. The results showed that initial solution pH played a significant role in MB adsorption. The higher pH favored the adsorption process. The maximum adsorption capacity reached 128.2 mg g^{-1}. The adsorption followed pseudo-second-order kinetics. The Frundlich and Temkin isotherms showed the highest correlation with experimental data for the MB adsorption. The MB adsorption process was well described by the Boyd's film-diffusion, indicating that the mechanism of MB adsorption by OASMS is the external mass transfer. Thermodynamic parameters indicated that the adsorption process is exothermic, feasible, and spontaneous. The results showed that OASMS is a potential adsorbent for treatment of wastewater containing MB.

Acknowledgment

This work was financially supported by the Fundamental Research Funds for the Central Universities [DL12DB04].

References

[1] N. Mohan, N. Balasubramanian, C.A. Basha, Electrochemical oxidation of textile wastewater and its reuse, J. Hazard. Mater. 147 (2007) 644–651.
[2] R. Malik, D.S. Ramteke, S.R. Wate, Adsorption of malachite green on groundnut shell waste based powdered activated carbon, Waste Manage. 27 (2007) 1129–1138.
[3] K. Kadirvelu, M. Kavipriya, C. Karthika, M. Radhika, N. Vennilamani, S. Pattabhi, Utilization of various agricultural wastes for activated carbon preparation and application for the removal of dyes and metal ions from aqueous solutions, Bioresour. Technol. 87 (2003) 129–132.
[4] V. Garg, Basic dye (methylene blue) removal from simulated wastewater by adsorption using Indian rosewood sawdust: A timber industry waste, Dyes Pigm. 63 (2004) 243–250.
[5] T. Robinson, G. McMullan, R. Marchant, P. Nigam, Remediation of dyes in textile effluent: A critical review on current treatment technologies with a proposed alternative, Bioresour. Technol. 77 (2001) 247–255.
[6] M.T. Sulak, E. Demirbas, M. Kobya, Removal of Astrazon yellow 7GL from aqueous solutions by adsorption onto wheat bran, Bioresour. Technol. 98 (2007) 2590–2598.
[7] R. Qadeer, Adsorption behavior of ruthenium ions on activated charcoal from nirtic acid medium, Colloids Surf. A: Physicochem. Eng. Aspects 293 (2007) 217–223.
[8] V.C. Srivastava, I.D. Mall, I.M. Mishra, Adsorption thermodynamics and isosteric heat of adsorption of toxic metal ions onto bagasse fly ash (BFA) and rice husk ash (RHA), Chem. Eng. J. 132 (2007) 267–278.

[9] P. Nigam, G. Armour, I.M. Banat, D. Singh, R. Marchant, Physical removal of textile dyes from effluents and solid-state fermentation of dye-adsorbed agricultural residues, Bioresour. Technol. 72 (2000) 219–226.
[10] T. Robinson, B. Chandran, P. Nigam, Removal of dyes from an artificial textile dye effluent by two agricultural waste residues, corncob and barley husk, Environ. Int. 28 (2002) 29–33.
[11] Z. Aksu, I.A. Isoglu, Use of agricultural waste sugar beet pulp for the removal of Gemazol turquoise blue-G reactive dye from aqueous solution, J. Hazard. Mater. 137 (2006) 418–430.
[12] V.K. Gupta, R. Jain, S. Varshney, Removal of Reactofix golden yellow 3 RFN from aqueous solution using wheat husk—An agricultural waste, J. Hazard. Mater. 142 (2007) 443–448.
[13] M. Doğan, H. Abak, M. Alkan, Biosorption of methylene blue from aqueous solutions by hazelnut shells: Equilibrium, parameters and isotherms, Water Air, and Soil Pollut. 192 (2008) 141–153.
[14] B.H. Hameed, A.A. Ahmad, Batch adsorption of methylene blue from aqueous solution by garlic peel, an agricultural waste biomass, J. Hazard. Mater. 164 (2009) 870–875.
[15] C.T. Weber, E.L. Foletto, L. Meili, Removal of Tannery Dye from aqueous solution using papaya seed as an efficient natural biosorbent, Water Air Soil Pollut. 224 (2013) 1427–1437.
[16] E.K. Mitter, C.R. Corso, FT-IR analysis of acid black dye biodegradation using saccharomyces cerevisiae immobilized with treated sugarcane bagasse, Water Air Soil Pollut. 224 (2013) 1607–1615.
[17] X. Yu, G. Zhang, C. Xie, Y. Yu, T. Cheng, Q. Zhou, Equilibrium, kinetic, and thermodynamic studies of hazardous dye neutral red biosorption by spent corncob substrate, BioResources 6 (2011) 936–949.
[18] S. Nethaji, A. Sivasamy, R.V. Kumar, A.B. Mandal, Preparation of char from lotus seed biomass and the exploration of its dye removal capacity through batch and column adsorption studies, Environ. Sci. Pollut. Res. 20 (2013) 3670–3678.
[19] S. Lagergren, Zur theorie der sogenannten adsorption geloster stoffe [The theory of the so-called adsorption of dissolved materials], Vetenskapsakad. Handl. 24 (1898) 1–39.
[20] Y.S. Ho, G. McKay, Pseudo-second order model for sorption processes, Process Biochem. 34 (1999) 451–465.
[21] W.J. Weber, J.C. Morriss, Kinetics of adsorption on carbon from solution, J. Sanit. Eng. Div. Am. Soc. Civil Eng. 89 (1963) 31–60.
[22] G.E. Boyd, A.W. Adamson, L.S. Myers, The exchange adsorption of ions from aqueous solutions by organic zeolites. II. Kinetics 1, J. Am. Chem. Soc. 69 (1947) 2836–2848.
[23] B. Tang, Y. Lin, P. Yu, Y. Luo, Study of aniline/-caprolactam mixture adsorption from aqueous solution onto granular activated carbon: Kinetics and equilibrium, Chem. Eng. J. 187 (2012) 69–78.
[24] G.F. Malash, M.I. El-Khaiary, Piecewise linear regression: A statistical method for the analysis of experimental adsorption data by the intraparticle-diffusion models, Chem. Eng. J. 163 (2010) 256–263.
[25] D. Reichenberg, Properties of ion-exchange resins in relation to their structure. III. Kinetics of exchange, J. Am. Chem. Soc. 75 (1953) 589–597.
[26] W.S. Alencar, E. Acayanka, E.C. Lima, B. Royer, F.E. de Souza, J. Lameira, C.N. Alves, Application of *Mangifera indica* (mango) seeds as a biosorbent for removal of Victazol Orange 3R dye from aqueous solution and study of the biosorption mechanism, Chem. Eng. J. 209 (2012) 577–588.
[27] I. Langmuir, The adsorption of gases on plane surfaces of glass, mica and platinum, J. Am. Chem. Soc. 40 (1918) 1361–1403.
[28] H.M.F. Freundlich, Uber die adsorption in losungen, J. Phys. Chem. 57 (1906) 385–470.
[29] M.J. Temkin, V. Pyzhev, Kinetics of ammonia synthesis on promoted iron catalysts, Acta Physiochim. URSS 12 (1940) 217–222.
[30] X. Han, W. Wang, X. Ma, Adsorption characteristics of methylene blue onto low cost biomass material lotus leaf, Chem. Eng. J. 171 (2011) 1–8.
[31] S.T. Akar, A. Gorgulu, Z. Kaynak, B. Anilan, T. Akar, Biosorption of reactive blue 49 dye under batch and continuous mode using a mixed biosorbent of macrofungus Agaricus bisporus and Thuja orientalis cones, Chem. Eng. J. 148 (2009) 26–34.
[32] S.J. Canete, Z. Zhang, L. Kong, V.L. Schlegel, B.A. Plantz, P.A. Dowben, R.Y. Lai, Application of synchrotron FTIR microspectroscopy for determination of spatial distribution of methylene blue conjugated onto a SAM via "click" chemistry, Chem. Commun. 47 (2011) 11918–11920.
[33] A.Y. Dursun, O. Tepe, G. Uslu, G. Dursun, Y. Saatci, Kinetics of remazol black B adsorption onto carbon prepared from sugar beet pulp, Environ. Sci. Pollut. Res. 20 (2013) 2472–2483.
[34] P. Senthil Kumar, S. Ramalingam, C. Senthamarai, M. Niranjanaa, P. Vijayalakshmi, S. Sivanesan, Adsorption of dye from aqueous solution by cashew nut shell: Studies on equilibrium isotherm, kinetics and thermodynamics of interactions, Desalination 261 (2010) 52–60.
[35] N.K. Amin, Removal of direct blue-106 dye from aqueous solution using new activated carbons developed from pomegranate peel: Adsorption equilibrium and kinetics, J. Hazard. Mater. 165 (2009) 52–62.
[36] F.P. de Sá, B.N. Cunha, L.M. Nunes, Effect of pH on the adsorption of sunset yellow FCF food dye into a layered double hydroxide (CaAl-LDH-NO_3), Chem. Eng. J. 215–216 (2013) 122–127.
[37] M.I. El-Khaiary, G.F. Malash, Common data analysis errors in batch adsorption studies, Hydrometallurgy 105 (2011) 314–320.
[38] M.A. Rauf, S.B. Bukallah, F.A. Hamour, A.S. Nasir, Adsorption of dyes from aqueous solutions onto sand and their kinetic behavior, Chem. Eng. J. 137 (2008) 238–243.